Supplementary Materials for "Localization on a Synthetic Hall Cylinder"

Ren Zhang,[1,2] Yangqian Yan,[2] and Qi Zhou[2]

[1]School of Physics, Xi'an Jiaotong University, Xi'an, Shaanxi 710049

[2]Department of Physics and Astronomy, Purdue University, West Lafayette, Indiana, 47907

(Dated: April 18, 2021)

Absence of the intrinsic lattice on a Hall ribbon

In this section, we show that the periodic boundary along the synthetic dimension is necessary for the presence of the intrinsic lattice, and hence the delocalization-localization transition when the external lattice is turned on. For simplicity, we start with the case that there are three site along the synthetic dimension, i.e., $N=3$, which is considered in the main text. We express the Hamiltonian in Eq.(1) in the main text into a matrix form as follows

$$\hat{H}_0=\begin{pmatrix} \frac{\hat{p}^2}{2m}+\epsilon_1 & 0 & 0 \\ 0 & \frac{\hat{p}^2}{2m}+\epsilon_2 & 0 \\ 0 & 0 & \frac{\hat{p}^2}{2m}+\epsilon_3 \end{pmatrix}+\begin{pmatrix} V\sin^2(k_Lx) & \frac{\Omega_1}{2}e^{2ik_0x+i\phi_1} & \frac{\Omega_3}{2}e^{-i\phi_3} \\ \frac{\Omega_1}{2}e^{-2ik_0x-i\phi_1} & V\sin^2(k_Lx) & \frac{\Omega_2}{2}e^{2ik_0x+i\phi_2} \\ \frac{\Omega_3}{2}e^{i\phi_3} & \frac{\Omega_2}{2}e^{-2ik_0x-i\phi_2} & V\sin^2(k_Lx) \end{pmatrix}, \tag{S1}$$

where we have set $k_1=k_2=k_0, k_3=0$. It is clear that Ω_3 is the coupling strength between states $|1\rangle$ and $|3\rangle$ induced by the Raman laser. $\Omega_3=0$ and $\Omega_3\neq 0$ represent the open and period boundary condition, respectively. To obtain a more insightful form, we rotation the Hamiltonian in Eq.(S1) by the following transformation

$$\hat{U}=\begin{pmatrix} 1 & 0 & 0 \\ 0 & e^{-i(2k_0x+\phi_1)} & 0 \\ 0 & 0 & e^{-i(4k_0x+\phi_1+\phi_2)} \end{pmatrix}, \tag{S2}$$

then the rotated Hamiltonian is written as

$$\hat{H}_0'=\hat{U}^\dagger\hat{H}_0\hat{U}=\begin{pmatrix} \frac{\hat{p}^2}{2m}+\epsilon_1 & 0 & 0 \\ 0 & \frac{(\hat{p}-2k_0)^2}{2m}+\epsilon_2 & 0 \\ 0 & 0 & \frac{(\hat{p}-4\hbar k_0)^2}{2m}+\epsilon_3 \end{pmatrix}+\begin{pmatrix} V\sin^2(k_Lx) & \frac{\Omega_1}{2} & \frac{\Omega_3}{2}e^{-i(4k_0x+\phi)} \\ \frac{\Omega_1}{2} & V\sin^2(k_Lx) & \frac{\Omega_2}{2} \\ \frac{\Omega_3}{2}e^{i(4k_0x+\phi)} & \frac{\Omega_2}{2} & V\sin^2(k_Lx) \end{pmatrix}, \tag{S3}$$

where $\phi=\sum_{j=1}^{j=3}\phi_j$. Then it becomes evident that under the open boundary condition, i.e., $\Omega_3=0$, the accumulated phase associated with the Raman laser can be gauged away, and the Hamiltonian in Eq.(S3) describe the spin-orbit coupling atoms in an external lattice $V\sin^2(k_Lx)$. In such case, the system is continuously translational symmetric, and the ground state density distribution should be uniform. In the presence of external lattice, even the density distribution then becomes periodic, no localization occurs.

In Fig. S1, we show the low-energy spectrum and the ground state density distribution. In our calculation for the energy spectrum, we use the periodic boundary condition in the synthetic dimension and take $\Omega_1=\Omega_2=\Omega_3=\Omega$. Our results show that even in the absence of the external lattice, the band structure appears , which is the character of the periodic potential, as illustrated in Fig. S1(a,b) with different Ω. This is one of the manifestations of the intrinsic lattice. The intrinsic lattice is more explicitly manifested in the density distribution, as shown in Fig. S1(d,e). Under the periodic boundary condition, the density distribution is periodic as shown by the solid blue curves, the same as that in the presence of a periodic lattice. Moreover, we find the amplitude increases when Ω becomes larger, while the period remains. This implies that the depth of the intrinsic lattice is determined by the Raman coupling strength Ω, and the period is determined by the transferred momentum after a closed loop in the synthetic dimension. Here, the transferred momentum is $2k_0$, hence the period of the intrinsic lattice is $d_I=\pi/2k_0$. However, under the open boundary condition, the density distribution is uniform, the same as that in the free space, as shown by the purple lines. This phenomenon explicitly demonstrates that the periodic boundary condition along the synthetic dimension is of fundamental importance to the intrinsic lattice in the real dimension. We also show the results when the external lattice is turned on in Fig. S1(c,f). We find that the Brillouin zone folds as expected, since the period the composite lattice enlarges. Correspondingly, the density distribution becomes more involved, like that in a random potential. However, under the open boundary condition, the wave function is still delocalized as shown by the dashed line in Fig. S1(f).

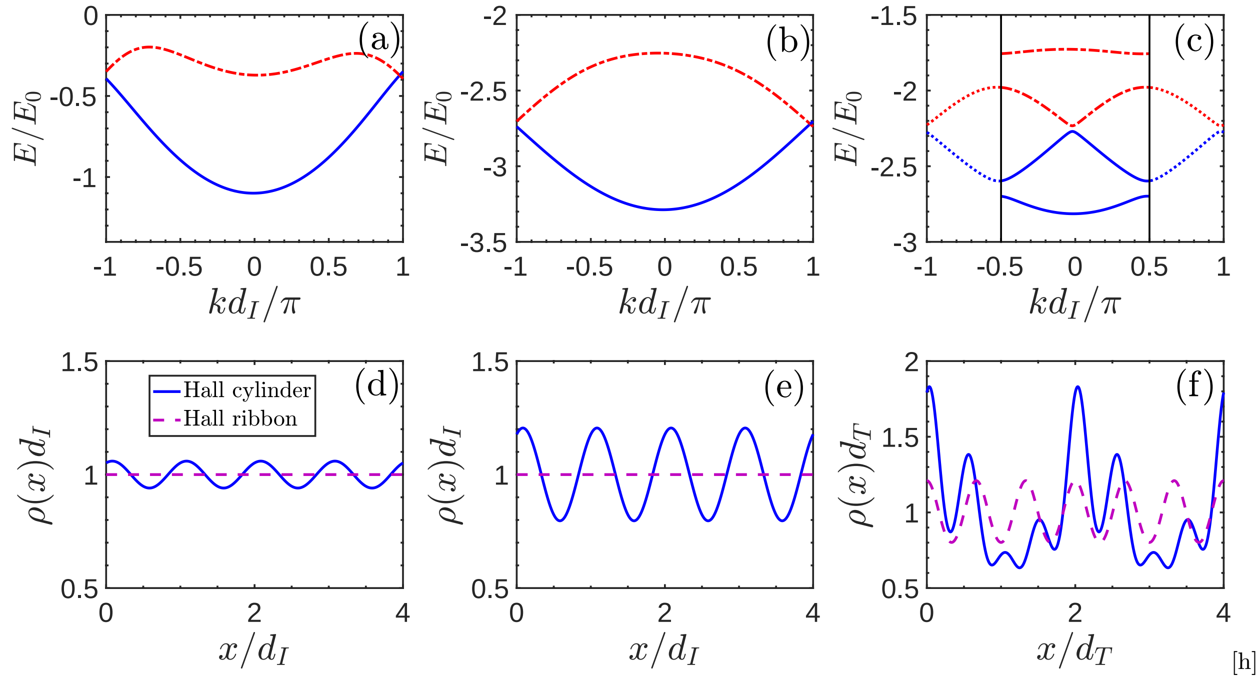

FIG. S1. Energy spectrum and density distribution. A few energy bands in Hall cylinder without (a,b) and with (c) the external optical lattice. (c): Ground state density distribution $\rho(x) = \sum_{j=1}^{3} |\psi_j(x)|^2$ in Hall cylinder and Hall ribbon without (d,e) and with (f) the external lattice. The energy unit is defined as $E_0 = \hbar^2 k_0^2/2m$. The density distributions in two unit cells are shown. In our calculation, the parameters are taken as follows: $\epsilon_1 = -0.1E_0$, $\epsilon_2 = 0$, $\epsilon_3 = 0.1E_0$, $\phi_1 = \pi/3$, $\phi_2 = \pi/2$ and $k_L/k_0 = 5/3$, and (a,d): $V = 0E_0$, $\Omega = 2E_0$; (b,e): $V = 0E_0$, $\Omega = 5E_0$; (c,f): $V = 1E_0$, $\Omega = 5E_0$. d_I and d_T are the spatial period of the intrinsic lattice and the composite lattice, respectively.

Equation (S3) also tells us that, when the external lattice is absent, i.e., $V = 0$, ϕ simply determines the origin of the intrinsic lattice, as it can be adsorbed by re-defining x as $x - \phi/(4k_0)$. As such, in an infinite system with translational symmetry, ϕ does not affect any physical quantities.

For a general case with $N > 3$, it can also be verified that the phase associated with Raman laser can also be gauged away under the open boundary condition. To be specific, we define the unitary operator as follows

$$\hat{U}_{mn} = \begin{cases} e^{-i(2(n-1)k_0 x + \theta_n)}; & m = n \\ 0; & \text{otherwise} \end{cases}, \tag{S4}$$

where $\theta_n = -\sum_{i=0}^{n-1} \phi_i$, and the rotated Hamiltonian $\hat{H}_0' = \hat{U}^\dagger \hat{H}_0 \hat{U}$ has the position dependent off-diagonal term

$$\hat{H}_{1N}' = \frac{\Omega_N}{2} e^{-i(2(N-1)k_0 x + \phi)}, \tag{S5}$$

which characterize the boundary condition along the synthetic dimension. All other off-diagonal terms are position independent. As such, there is no intrinsic lattice when $\Omega_N = 0$, i.e., under the open boundary condition, and the delocalization-localization transition does not occur even with the external lattice. We would like to point out that whereas the periodic boundary condition gives rise to the density modulation in the real dimension for any N, increasing N leads to smaller modulation amplitudes on the Hall cylinder. This is because of the kinetic energy cost in the Raman transition that flips the spins and meanwhile changes the momentum. The larger N is, more states with different energies will be involved. As such, increasing N shall increase the total energy barrier for the atom to return to the original spin state and the amplitude of the intrinsic lattice will be suppressed.

Delocalization-localization transition for different wavenumber ratios

In this section, we present how the boundary between the delocalized state and the localized state transition builds up when varying the wavenumber ratios. As stated in the main text, we approach the gold number using the Fibonacci series and calculate the inverse participation ratio (IPR) defined in Eq.(5) of the main text.

In Fig. S2, we present the delocalization-localization transition for different wavenumber ratios $k_L/2k_0$. Comparing the IPR in Fig. S2 (a,b,c), we find that as the wavenumber ratio approaches the irrational number (golden number here), the arc-like boundary between the delocalized state and the localized state becomes clearer and clearer. To be specific, let us consider one particular $V/E_0 = 10$ and ramps the Raman laser up from zero under varying wavenumber ratio $k_L/2k_0$, as illustrated by the red dashed curves. When $k_L/2k_0 = 5/3$ (rational number), the IPR grows continuously when Ω increases, as shown in Fig. S2(d). By change the wavenumber ratio to $k_L/2k_0 = 21/13$, we see the IPR grows dramatically around $\Omega/E_0 \approx 3$ and smoothly elsewhere, as shown in Fig. S2(e). Further changing $k_L/2k_0 = 55/34$ which a good approximation for the golden ratio, we find the IPR almost jumps around $\Omega/E_0 \approx 3$, as shown in Fig. S2(f). As such, it is reasonable to expect a sharp delocalization-localization transition when a wavenumber ratio is an irrational number, and an arc-like delocalization-localization boundary appears in the V-Ω plane. The corresponding density distribution in real space is shown in Fig. S2 (g,h,i). It is obvious that when the wavenumber ratio approaches an irrational number, the density distribution in real space becomes more and more localized.

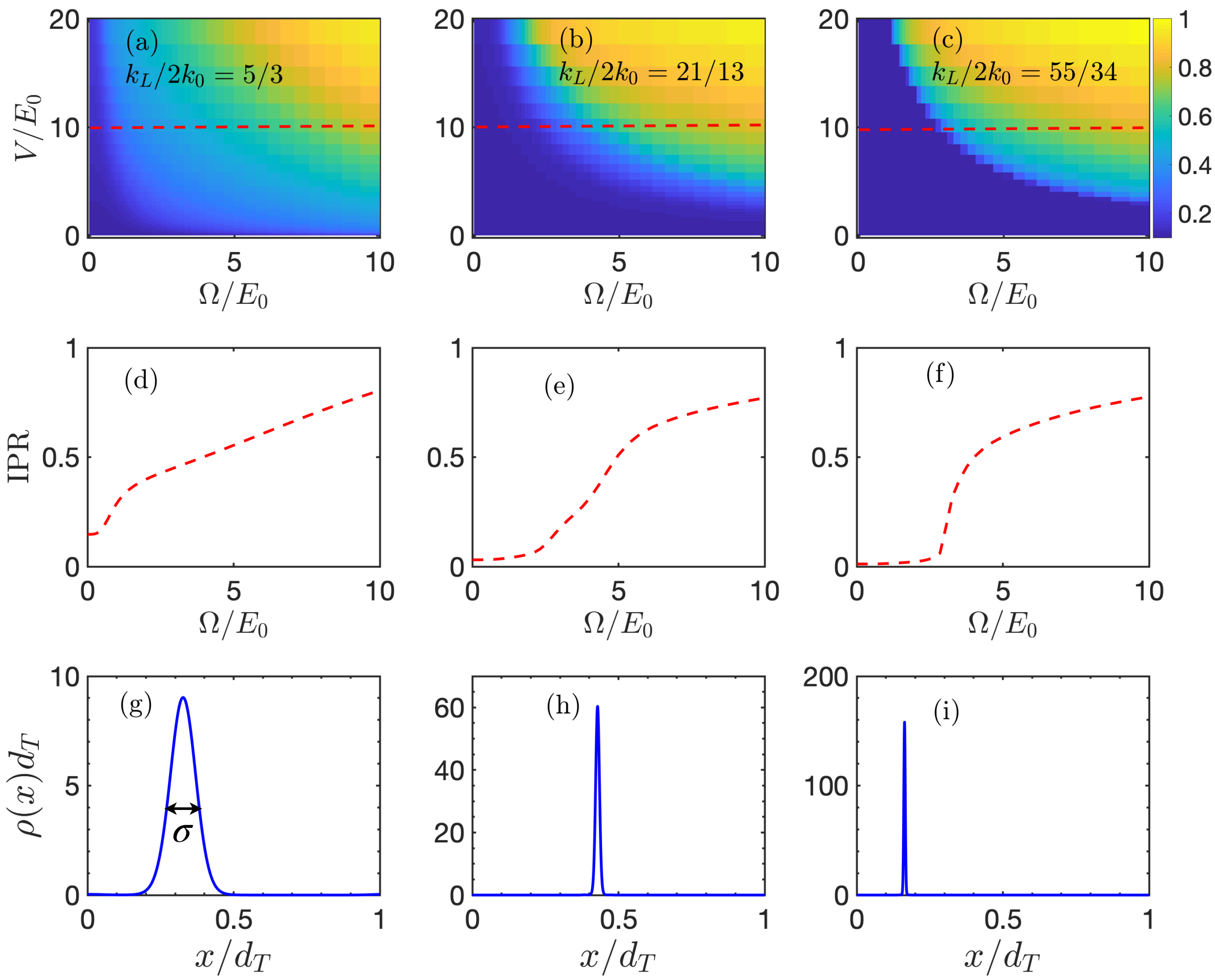

FIG. S2. Delocalization-localization transition for varying wavenumber ratios $k_L/2k_0$. The energy unit is the recoil energy of the Raman laser defined as $E_0 = \hbar^2 k_0^2/2m$. Color bar in (a,b,c) denotes the value of the IPR. In our calculation, the parameters are taken as follows: $\epsilon_1 = -0.1E_0$, $\epsilon_2 = 0$, $\epsilon_3 = 0.1E_0$, $\phi_1 = \pi/3$, $\phi_2 = \pi/2$. The red dashed lines in (a,b,c) are used to guide eyes. The IPR for $V = 10E_0$ are shown in (d,e,f). In (g,h,i), we present the density distribution in real dimension, and in our calculation $V = 20E_0, \Omega = 10E_0$.

We would like to point out that there is no threshold of the localization to delocalization transition shown in Fig. S2 (c). Using $\tilde{V}(\Omega)$ to denote the arc-like boundary between the localized and delocalized states, $\tilde{V}(\Omega)$ monotonically decreases with increasing Ω. In other words, the boundary will asymptotically be close to the V-axis when Ω decreases down to zero, which means that the required Raman coupling strength is infinitesimal when the external lattice is infinitely strong. This can be understood from the fact that the tunneling amplitude in an extremely deep external lattice alone is so small that a very weak intrinsic lattice is sufficient to drive the system to the localized regime. Similarly, the boundary will be asymptotically close to the Ω-axis when Ω/E_0 approaches infinity. This time, the tunneling created by an extremely deep intrinsic lattice is so small that an infinitesimal external lattice can turn the states into localized ones.

Mobility edge and energy spectra on the synthetic Hall cylinder

In this section, we discuss IPR of the whole energy spectrum and how does the energy spectrum depends on the distribution of the synthetic magnetic field on the Hall cylinder. To quantify the localization of the entire spectrum, we define the IPR for each state as follows

$$\mathrm{IPR}(i) = \frac{\int_0^{d_T} dx \left[\sum_{j=1}^{3} |\psi_j^{(i)}(x)|^2\right]^2}{k_0 \left[\int_0^{d_T} dx \sum_{j=1}^{3} |\psi_j^{(i)}(x)|^2\right]^2}. \tag{S6}$$

where $\psi_j^{(i)}(x)$ is the j-component of the i-th eigenstate.

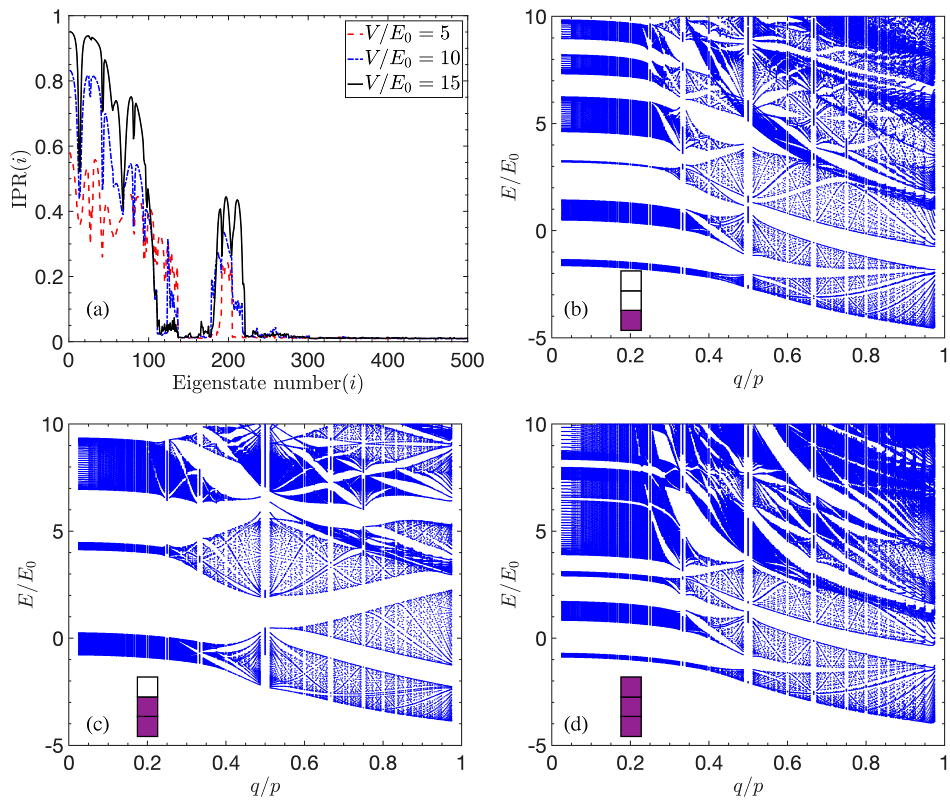

FIG. S3. Mobility edge (a) and energy spectra (b, c, d) on the synthetic Hall cylinder. In our calculation, the parameters are taken as follows: (a): $\Omega = 10E_0, \epsilon_1 = -0.1E_0$, $\epsilon_2 = 0$, $\epsilon_3 = 0.1E_0$, $\phi_1 = \pi/3$, $\phi_2 = \pi/2$. (b, c, d): $\Omega = 8E_0, V = 10E_0, \epsilon_1 = -0.1E_0$, $\epsilon_2 = 0$, $\epsilon_3 = 0.1E_0$, $\phi_1 = \phi_2 = 0$. The purple rectangle denotes a finite synthetic magnetic flux per plaquette, and the white rectangle denotes a vanishing flux.

In Fig. S3(a), we calculate IPR for the 500 eigenstates. Several important features are noticeable. (1): It is apparent that from $\sim$220th eigenstate, the IPR for the higher excited state is near zero, which means these states are delocalized, no matter whether the ground state is localized or delocalized. The $\sim$220th state serves as a mobility edge on the synthetic Hall cylinder. (2): For states in $[1, \sim 120]$, the IPR is finite, which means the low-energy states can be localized, as denoted by the solid black curves, and the $\sim$120th state can be viewed as another mobility edge. (3): There exists an isolated regime around $[180, 200]$ where the IPR is finite. So, we conclude that there are two localized regimes. One is near the ground state and the other one is embedded into the highly excited spectrum.

The energy spectrum on the Hall cylinder shows a rich structure by changing q/p. This is similar to that of the energy spectrum of the Hofstadter model by tuning the magnetic flux per plaquette, as shown in Fig. S3(b,c,d) reminiscent of the Hofstadter butterfly. Moreover, thanks to the flexibility of the Raman coupling scheme, the synthetic magnetic flux on the Hall cylinder can be made uniform or highly non-uniform. For instance, as illustrated in Fig. S3(b), $1/3$ of the cylindrical surface, which corresponds to the Raman coupling between states $|1\rangle$ and $|2\rangle$, is penetrated by a synthetic magnetic field, while the remaining $2/3$, which corresponds to the microwave coupling between states $|2\rangle$ and $|3\rangle$, $|3\rangle$ and $|1\rangle$, is not. Similarly, $2/3$ of the cylindrical surface can be penetrated by a synthetic magnetic field, and the remaining $1/3$ part is not penetrated by the synthetic magnetic field, as shown in Fig. S3(c). The cylindrical surface can be uniformly penetrated by a synthetic magnetic field, as shown in Fig. S3(d). It is clear that the spectrum changes for different coupling schemes, which provides experimentalists a new means to engineer the energy spectrum.

The variance of IPR

As we state in the main text, the constant Raman laser phase ϕ may fluctuate in repeated experiments, and the dependence of IPR on ϕ is profound near the delocalization-localization transition. In Fig. 4(b,d), we have illustrated this phenomenon by using two different ϕ. To be more explicit, we calculate the variance of IPR

$$\mathrm{Var(IPR)} = \frac{1}{N-1}\sum_{i=1}^{N} |\mathrm{IPR}(\phi_\mathrm{i}) - \langle \mathrm{IPR} \rangle|^2, \tag{S7}$$

where N denotes the number of ϕ_i, and $\langle \mathrm{IPR} \rangle$ is the mean of the IPR. The dependence of Var(IPR) on Ω is shown in Fig. S4. It is clear that the variance of IPR is maximized near the delocalization-localization transition, which is consistent with the conclusion in the main text. Hence, the variance of the IPR peak can be used to indicate the transition point.

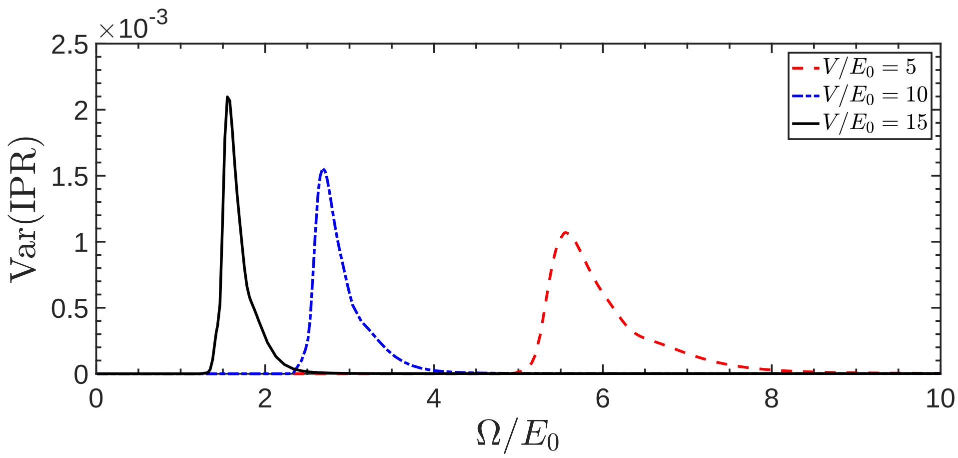

FIG. S4. Variance of the IPR across the delocalization-localization transition on Hall cylinder. In our calculation, the parameters are taken as follows: $\epsilon_1 = -0.1E_0$, $\epsilon_2 = 0$, $\epsilon_3 = 0.1E_0$, $l = 9$.

Robustness to weak interaction

In current experiments, the background interaction is usually very weak. In the main text, we show that the delocalization to localization transition is robust to the weak interaction. Here, we use Rb and Na atomic gas in 3D trap as examples to estimate the interaction strength. A straightforward derivation finds $gn/E_0 = 8\pi a_s n/k_0^2$, where a_s is the s-wave scattering length, n is the particle number density. $k_0 = 2\pi/\lambda$ is the wave number of the Raman laser with wave length λ. The typical density in cold atomic gas is around $n \sim 10^{13}\mathrm{cm}^{-3}$ and the Raman laser wave length is about $\lambda = 1064$nm. The background scattering length for Rb and Na are about $100a_0$ and $60a_0$, respectively, with a_0 being the Bohr's radius [1]. Then we find $gn/E_0 \approx 0.038$ for Rb and $gn/E_0 \approx 0.023$ for Na, which means the interaction can be viewed as a weak perturbation. For the 1D case which is far away from a confinement induced resonance, the interaction strength $g_{1D} \approx \int d\rho g |\psi_\perp(\rho)|^2$, and the 1D number density $n_{1D} \approx \int d\rho n/\psi_\perp(\rho)|^2$, where $\psi_\perp(\rho)$ denote the wave function on the radial direction. As such, under this approximation, the interaction strength is of the same order as that in 3D, and can also be viewed as a weak perturbation in 1D. On the other hand, there are tools to tune the interaction in cold atom systems, for instance, Feshbach resonance [1] and confinement induced resonance [2]. Utilizing these resonances, the interaction can be tuned to be zero. Thus, the localization illustrated in our main text can also well exhibit itself even the background interaction is not so weak.

[1] C. Chin, R. Grimm, P. Julienne, and E. Tiesinga, Feshbach resonances in ultracold gases, Rev. Mod. Phys. **82**, 1225 (2010).

[2] M. Olshanii, Atomic scattering in the presence of an external confinement and a gas of impenetrable bosons, Phys. Rev. Lett. **81**, 938 (1998).